

Training Deep Learning based Denoisers without Ground Truth Data

Shakarim Soltanayev¹ Se Young Chun¹

Abstract

Recent deep learning based denoisers are trained to minimize the mean squared error (MSE) between the output of a network and the ground truth noiseless image in the training data. Thus, it is crucial to have high quality noiseless training data for high performance denoisers. Unfortunately, in some application areas such as medical imaging, it is expensive or even infeasible to acquire such a clean ground truth image. We propose a Stein’s Unbiased Risk Estimator (SURE) based method for training deep learning based denoisers without ground truth data. We demonstrated that our SURE based method only with noisy input data was able to train CNN based denoising networks that yielded performance close to that of the original MSE based deep learning denoisers with ground truth data.

1. Introduction

Deep learning has been successful in various high-level computer vision tasks (LeCun et al., 2015) such as image classification (Krizhevsky et al., 2012; He et al., 2016), object detection (Girshick et al., 2014; Ren et al., 2015), and semantic segmentation (Chen et al., 2015; Long et al., 2015). Deep learning has also been investigated for low-level computer vision tasks such as image denoising (Vincent et al., 2010; Burger et al., 2012; Wang & Morel, 2014; Zhang et al., 2017a; Lefkimiatis, 2017), image inpainting (Xie et al., 2012), and image restoration (Mao et al., 2016; Gao & Grauman, 2017; Zhang et al., 2017b). In particular, image denoising is a fundamental computer vision task that does not only yield a clean image with reduced noise, but also improves other tasks such as image classification (Vincent et al., 2010) and image restoration (Zhang et al., 2017b).

Deep learning based image denoisers have been investigated (Burger et al., 2012; Zhang et al., 2017a; Lefkimiatis, 2017) and have yielded performance equivalent to

or better than conventional state-of-the-art denoising techniques such as BM3D (Dabov et al., 2007). These deep learning based denoisers train their networks by minimizing the mean squared error (MSE) between the output of a network and the target noiseless image. Thus, it is crucial to have high quality noiseless images for high performance deep learning denoisers.

High quality camera sensors and abundant light allows to obtain high quality, almost noiseless 2D images in daily environment. Acquiring such a high quality photo is quite cheap due to smart phones and digital cameras. However, in some application areas such as medical imaging, acquiring almost noiseless ground truth data for training is expensive or sometimes even infeasible.

In X-ray CT (Computed Tomography), Poisson noise is added in the measurement domain. This noise can be reduced by increasing radiation dose, but high dose will lead to harmful effect on scanned subjects and too high dose may saturate CT detectors (*e.g.*, similar to taking a photo of sun without any filter). Recent works on deep learning based image denoisers (Chen et al., 2017; Kang et al., 2017; Wolterink et al., 2017) utilized normal dose CT images as ground truth so that denoising networks are trained to yield images with normal dose level noise instead of noiseless image. Similarly, there have been some works to predict standard dose PET (Positron Emission Tomography) image from low dose PET image as well as additional anatomical side information (Wang et al., 2016). Increasing radiation dose in PET usually leads to higher risk for patients and increased detector dead time (data in dead time window can not be used). Thus, it is infeasible to obtain noiseless PET images in general. In other medical imaging modalities such as MRI (Magnetic Resonance Imaging) or ultrasound, it is challenging or expensive to obtain noiseless images, particularly for high resolution settings.

Conventional denoising methods usually do not require noiseless ground truth images to perform denoising, but often require tuning parameters of image filters for the best possible results (minimum MSE). Since there is no noiseless ground truth images for the noisy input image, there have been several works of using Stein’s Unbiased Risk Estimator (SURE) (Stein, 1981) to find the optimal parameters. For instance, Ramani *et al.* proposed a Monte-Carlo

¹Department of Electrical Engineering, Ulsan National Institute of Science and Technology (UNIST), Ulsan, Republic of Korea. Correspondence to: Se Young Chun <sychun@unist.ac.kr>.

based SURE method to determine near optimal denoising parameters (Ramani et al., 2008). There have been a few works (Van De Ville & Kocher, 2009; Salmon, 2010; Van De Ville & Kocher, 2011) on SURE based methods to optimize the parameters of popular NLM (Non-Local Means) filter (Buades et al., 2005). Since SURE, an unbiased estimator of MSE, does not require to use ground truth data, these methods can be used to optimize filter parameters only with noisy input data.

As an initial step toward training deep learning based denoisers without ground truth data for medical imaging, we investigated SURE based training methods for deep learning based denoisers. In Section 2, we review major results of SURE and Monte-Carlo SURE. Then, in Section 3, we describe our proposed training method using Monte-Carlo SURE for deep learning based image denoisers. In Section 4, denoising results are presented for BM3D (conventional state-of-the-art denoiser), deep learning based denoiser (stacked denoising autoencoder, U-Net and DnCNN-S) with MSE and the same deep learning denoiser with the proposed Monte-Carlo SURE training. Lastly, in Section 5, we conclude this paper by discussing several issues for our proposed method to be used for medical imaging.

2. Background

2.1. Stein's Unbiased Risk Estimator

The signal (or image) with Gaussian noise can be modeled:

$$\mathbf{y} = \mathbf{x} + \mathbf{n} \quad (1)$$

where $\mathbf{x} \in \mathbb{R}^K$ is an unknown signal following $\mathbf{x} \sim p(\mathbf{x})$, $\mathbf{y} \in \mathbb{R}^K$ is a known measurement and $\mathbf{n} \in \mathbb{R}^K$ is an *i.i.d.* Gaussian noise such that $\mathbf{n} \sim \mathcal{N}(\mathbf{0}, \sigma^2 \mathbf{I})$ and \mathbf{I} is an identity matrix. We denote $\mathbf{n} \sim \mathcal{N}(\mathbf{0}, \sigma^2 \mathbf{I})$ as $\mathbf{n} \sim \mathcal{N}_{0, \sigma^2}$.

An estimator of \mathbf{x} from \mathbf{y} (or denoiser) can be defined as a function of \mathbf{y} such that

$$\mathbf{h}(\mathbf{y}) = \mathbf{y} + \mathbf{g}(\mathbf{y}) \quad (2)$$

where \mathbf{h}, \mathbf{g} are functions from \mathbb{R}^K to \mathbb{R}^K . Then, a SURE for $\mathbf{h}(\mathbf{y})$ can be defined as follows:

$$\begin{aligned} \eta(\mathbf{h}(\mathbf{y})) &= \sigma^2 + \frac{\|\mathbf{g}(\mathbf{y})\|^2}{K} + \frac{2\sigma^2}{K} \sum_{i=1}^K \frac{\partial \mathbf{g}_i(\mathbf{y})}{\partial \mathbf{y}_i} \quad (3) \\ &= \frac{\|\mathbf{y} - \mathbf{h}(\mathbf{y})\|^2}{K} - \sigma^2 + \frac{2\sigma^2}{K} \sum_{i=1}^K \frac{\partial \mathbf{h}_i(\mathbf{y})}{\partial \mathbf{y}_i} \end{aligned}$$

where $\eta : \mathbb{R}^K \rightarrow \mathbb{R}$ and \mathbf{y}_i is the *i*th element of \mathbf{y} . Then, for a fixed \mathbf{x} , the following theorem holds:

Theorem 1. (Stein, 1981; Blu & Luisier, 2007) The random variable $\eta(\mathbf{h}(\mathbf{y}))$ is an unbiased estimator of

$$\text{MSE}(\mathbf{h}(\mathbf{y})) = \frac{1}{K} \|\mathbf{x} - \mathbf{h}(\mathbf{y})\|^2$$

or

$$\mathbb{E}_{\mathbf{n} \sim \mathcal{N}_{0, \sigma^2}} \left\{ \frac{\|\mathbf{x} - \mathbf{h}(\mathbf{y})\|^2}{K} \right\} = \mathbb{E}_{\mathbf{n} \sim \mathcal{N}_{0, \sigma^2}} \{ \eta(\mathbf{h}(\mathbf{y})) \} \quad (4)$$

where $\mathbb{E}_{\mathbf{n} \sim \mathcal{N}_{0, \sigma^2}} \{ \cdot \}$ is the expectation in terms of the random vector \mathbf{n} . Note that in Theorem 1, \mathbf{x} is treated as a fixed, deterministic vector.

In practice, σ^2 can be easily estimated (Ramani et al., 2008) and $\|\mathbf{y} - \mathbf{h}(\mathbf{y})\|^2$ only requires the output of the estimator (or denoiser). The last divergence term of (3) can be obtained analytically for some special cases such as linear filters or NLM filters (Van De Ville & Kocher, 2009; 2011). However, it is challenging to calculate this term for more general denoising methods analytically.

2.2. Monte-Carlo Stein's Unbiased Risk Estimator

Ramani et al. introduced a fast Monte-Carlo approximation of the divergence term in (3) for general denoisers. For a fixed unknown true image \mathbf{x} ,

Theorem 2. (Ramani et al., 2008) Let $\tilde{\mathbf{n}} \sim \mathcal{N}_{0, 1} \in \mathbb{R}^K$ be independent of \mathbf{n} or \mathbf{y} . Then,

$$\sum_{i=1}^K \frac{\partial \mathbf{h}_i(\mathbf{y})}{\partial \mathbf{y}_i} = \lim_{\epsilon \rightarrow 0} \mathbb{E}_{\tilde{\mathbf{n}}} \left\{ \tilde{\mathbf{n}}^t \left(\frac{\mathbf{h}(\mathbf{y} + \epsilon \tilde{\mathbf{n}}) - \mathbf{h}(\mathbf{y})}{\epsilon} \right) \right\} \quad (5)$$

provided that $\mathbf{h}(\mathbf{y})$ admits a well-defined second-order Taylor expansion. If not, this is still valid in the weak sense provided that $\mathbf{h}(\mathbf{y})$ is tempered.

Based on Theorem 2, the divergence term in (3) can be approximated with one realization of $\tilde{\mathbf{n}} \sim \mathcal{N}_{0, 1}$ and a fixed small positive value ϵ :

$$\frac{1}{K} \sum_{i=1}^K \frac{\partial \mathbf{h}_i(\mathbf{y})}{\partial \mathbf{y}_i} \approx \frac{1}{\epsilon K} \tilde{\mathbf{n}}^t (\mathbf{h}(\mathbf{y} + \epsilon \tilde{\mathbf{n}}) - \mathbf{h}(\mathbf{y})) \quad (6)$$

where t is a transpose operator. This expression has been shown to yield accurate unbiased estimate of MSE for many denoising methods $\mathbf{h}(\mathbf{y})$ (Ramani et al., 2008).

3. Method

In this section, we will develop our proposed Monte-Carlo SURE based training method for deep learning denoisers without noiseless ground truth images assuming Gaussian signal noise model in (1).

3.1. Training Denoisers using Stochastic Method

A typical risk for image denoisers with the signal generation model (1) is

$$\mathbb{E}_{\mathbf{x} \sim p(\mathbf{x}), \mathbf{n} \sim \mathcal{N}_{0, \sigma^2}} \|\mathbf{x} - \mathbf{h}(\mathbf{y}; \theta)\|^2 \quad (7)$$

where $\mathbf{h}(\mathbf{y}; \theta)$ is a deep learning based denoiser parametrized with a vector θ . It is usually infeasible to calculate (7) exactly due to expectation operator. Thus, the empirical risk for (7) is used as a cost function as follows:

$$\frac{1}{N} \sum_{j=1}^N \|\mathbf{h}(\mathbf{y}^{(j)}; \theta) - \mathbf{x}^{(j)}\|^2 \quad (8)$$

where $\{(\mathbf{x}^{(1)}, \mathbf{y}^{(1)}), \dots, (\mathbf{x}^{(N)}, \mathbf{y}^{(N)})\}$ are N number of training data, sampled from the joint distribution of $\mathbf{x}^{(j)} \sim p(\mathbf{x})$ and $\mathbf{n}^{(j)} \sim \mathcal{N}_{0, \sigma^2}$. Note that (8) is an unbiased estimator of (7).

To train the deep learning network $\mathbf{h}(\mathbf{y}; \theta)$ with respect to θ , a gradient based optimization algorithm is used such as stochastic gradient descent (SGD) (Bottou, 1998), momentum, Nesterov momentum (Nesterov, 1983), or Adam optimizer (Kingma & Ba, 2015). For any gradient based optimization method, it is essential to calculate the gradient of (7) with respect to θ as follows:

$$\mathbb{E}_{\mathbf{x} \sim p(\mathbf{x}), \mathbf{n} \sim \mathcal{N}_{0, \sigma^2}} 2 \nabla_{\theta} \mathbf{h}(\mathbf{y}; \theta)^t (\mathbf{h}(\mathbf{y}; \theta) - \mathbf{x}). \quad (9)$$

Therefore, it is sufficient to calculate the gradient of the empirical risk (8) to approximate (9).

In practice, calculating the gradient of (8) for large N is inefficient since a small amount of well-shuffled training data can approximate the gradient of (8) well. Thus, a mini-batch is used for efficient training by calculating the mini-batch empirical risk as follows:

$$\frac{1}{M} \sum_{j=1}^M \|\mathbf{h}(\mathbf{y}^{(j)}; \theta) - \mathbf{x}^{(j)}\|^2 \quad (10)$$

The equation (10) is still an unbiased estimator of (7) provided that the training data is randomly permuted every epoch and the same data is used no more than once per each epoch.

3.2. Proposed Training Method for Denoisers

To incorporate Monte-Carlo SURE into the stochastic approximation method for training, we modify (7) as

$$\mathbb{E}_{\mathbf{x} \sim p(\mathbf{x})} \left[\mathbb{E}_{\mathbf{n} \sim \mathcal{N}_{0, \sigma^2}} (\|\mathbf{x} - \mathbf{h}(\mathbf{y}; \theta)\|^2 | \mathbf{x}) \right]. \quad (11)$$

The equation (11) is equivalent to (7) due to conditioning.

From Theorem 1, an unbiased estimator for $\mathbb{E}_{\mathbf{n} \sim \mathcal{N}_{0, \sigma^2}} (\|\mathbf{x} - \mathbf{h}(\mathbf{y}; \theta)\|^2 | \mathbf{x})$ can be derived as

$$K \eta(\mathbf{h}(\mathbf{y}; \theta)) \quad (12)$$

such that for a fixed \mathbf{x}

$$\mathbb{E}_{\mathbf{n} \sim \mathcal{N}_{0, \sigma^2}} \|\mathbf{x} - \mathbf{h}(\mathbf{y}; \theta)\|^2 = K \mathbb{E}_{\mathbf{n} \sim \mathcal{N}_{0, \sigma^2}} \eta(\mathbf{h}(\mathbf{y}; \theta)).$$

Then, using the empirical risk expression in (10), an unbiased estimator for (7) is

$$\begin{aligned} & \frac{1}{M} \sum_{j=1}^M \|\mathbf{y}^{(j)} - \mathbf{h}(\mathbf{y}^{(j)}; \theta)\|^2 - K \sigma^2 \\ & + 2 \sigma^2 \sum_{i=1}^K \frac{\partial \mathbf{h}_i(\mathbf{y}^{(j)}; \theta)}{\partial \mathbf{y}_i} \end{aligned} \quad (13)$$

Note that there is no noiseless ground truth data $\mathbf{x}^{(j)}$ in (13).

Finally, the last divergence term in (13) can be approximated using Monte-Carlo SURE so that the final unbiased risk estimator for (7) will be

$$\begin{aligned} & \frac{1}{M} \sum_{j=1}^M \|\mathbf{y}^{(j)} - \mathbf{h}(\mathbf{y}^{(j)}; \theta)\|^2 - K \sigma^2 \\ & + \frac{2 \sigma^2}{\epsilon} (\tilde{\mathbf{n}}^{(j)})^t (\mathbf{h}(\mathbf{y}^{(j)} + \epsilon \tilde{\mathbf{n}}^{(j)}; \theta) - \mathbf{h}(\mathbf{y}^{(j)}; \theta)) \end{aligned} \quad (14)$$

where ϵ is a small fixed positive number and $\tilde{\mathbf{n}}^{(j)}$ is a single realization from the standard normal distribution for each training data j . In order to make sure that the estimator (14) is unbiased, the order of $\mathbf{y}^{(j)}$ should be randomly permuted and the new set of $\tilde{\mathbf{n}}^{(j)}$ should be generated every epoch.

The implementation of deep learning based image denoiser with the cost function of (14) can be done using deep learning development framework such as TensorFlow (Abadi et al., 2016) by defining the cost function properly. Then, the gradient of (14) can be automatically calculated when the training is performed.

One potential advantage of our SURE based training method is that we can use all available data without noiseless ground truth images. In other words, we can train denoising deep neural networks not only with training data, but also with test data together. This advantage may further improve the performance of deep learning based denoisers.

Lastly, almost any deep learning based image denoiser can utilize our Monte-Carlo SURE based training by modifying the cost function from (10) to (14) as far as it satisfies the condition in Theorem 2. Many deep learning based denoisers with differentiable activation functions (e.g., sigmoid) can meet this condition. Some denoisers with piecewise differentiable activation functions (e.g., ReLU) still make Theorem 2 in the weak sense since

$$\|\mathbf{h}(\mathbf{y}; \theta)\| \leq C_0 (1 + \|\mathbf{y}\|^{n_0})$$

for some $n_0 > 1$ and $C_0 > 0$. Therefore, we expect that our proposed method should work for most deep learning image denoisers (Vincent et al., 2010; Burger et al., 2012; Wang & Morel, 2014; Zhang et al., 2017a; Lefkimiatis, 2017).

4. Simulations

In this section, denoising simulation results with MNIST dataset using a simple stacked denoising autoencoder (SDA) (Vincent et al., 2010), CIFAR-10 dataset using a convolution-deconvolution deep network (U-NET) (Ronneberger et al., 2015), and natural image dataset using deep CNN (Convolutional Neural Network) image denoiser (DnCNN) (Zhang et al., 2017a) will be presented.

4.1. General Simulation Settings

All of the networks presented in this section (called NET, which can be one among SDA, U-NET, and DnCNN) were trained using one of the following two optimization objectives: (MSE) the minimum MSE between noisy input image and its ground truth image, (10); (SURE) the minimum Monte-Carlo SURE, (14). Note that ground truth images were not used in the latter case. For the training dataset, the following configuration were used:

- Training images corrupted by different realizations of Gaussian noise at each epoch (LG).
- Training images corrupted only once at the start of the training (SM).
- Training images corrupted once at the start of the training AND noisy images of test set (SM-T). This configuration is valid for SURE based methods.

Table 1 summarizes all simulated configurations including conventional state-of-the-art image denoiser, BM3D (Dabov et al., 2007), that does not require any training.

Table 1. Summary of denoising methods. NET can be one of the following deep learning based denoisers: SDA, U-Net, DnCNN.

METHOD	DESCRIPTION
BM3D	CONVENTIONAL METHOD
NET-MSE-LG	OPTIMIZING MSE WITH LG
NET-SURE-SM	OPTIMIZING SURE WITH SM
NET-SURE-SM-T	OPTIMIZING SURE WITH SM & T

4.2. Results: MNIST Dataset

We performed denoising simulations with MNIST dataset. The noisy images were generated based on the model (1) with two noise levels (one with standard deviation (SD) = 9.8% and the other with SD = 19.6%).

For the experiments on the MNIST dataset with 28×28 pixels, a simple SDA was chosen (Vincent et al., 2010). Decoder and encoder networks each consists of two convolutional layers (kernel size 3×3) with sigmoid activation functions each having a stride of 2 (both conv and conv

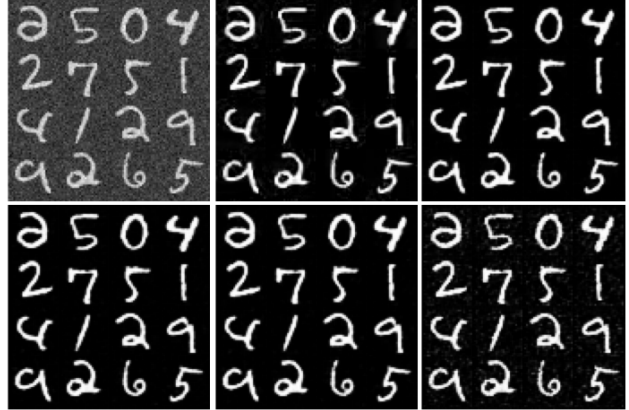


Figure 1. Results of denoising methods. From the top left, noisy image (SD = 9.8%), BM3D (row 1, center), SDA-MSE-LG (row 1, right), SDA-SURE-SM (row 2, left), SDA-SURE-SM-T (row 2, center), SDA-REG (row 2, right).

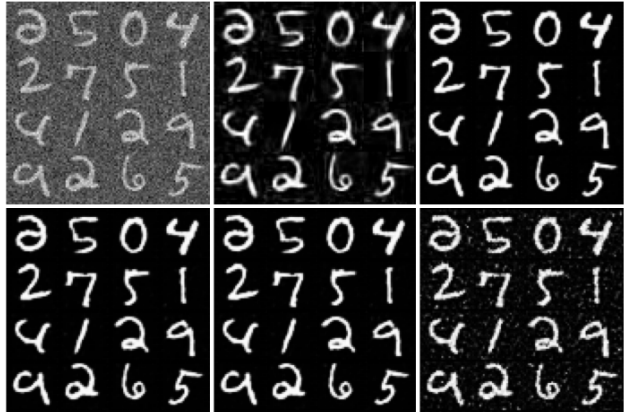


Figure 2. Results of denoising methods. From the top left, noisy image (SD = 19.6%), BM3D (row 1, center), SDA-MSE-LG (row 1, right), SDA-SURE-SM (row 2, left), SDA-SURE-SM-T (row 2, center), SDA-REG (row 2, right).

transposed). Thus, a training sample of size 28×28 is downsampled to 7×7 and then upsampled back to 28×28 .

SDA was trained to output a denoised image using a set of 55,000 training and 5,000 validation images. The performance of the model was tested with 100 images chosen randomly from the default test set of 10,000 images. For all cases SDA was trained with Adam optimizer (Kingma & Ba, 2015) with batch size of 200 and the learning rate of 0.001 for 100 epochs. The ϵ value in (6) was set to 0.0001.

Figure 1 illustrates the performance of different denoising methods. The subfigure at row 1, left is the noisy image contaminated with the noise level of SD = 9.8% and the subfigure at row 1, right is the denoising result of BM3D, which looks slightly blurrier than other results. Deep learning based denoising networks outperformed BM3D for all cases. However, it is hard to observe visually distinct results

Table 2. Results of deep learning based denoisers with different training configurations for MNIST (performance in dB). SURE based SDA denoisers yielded comparable to or better than MSE based SDA denoisers as well as BM3D.

METHOD	SD = 9.8%	SD = 19.6%
BM3D	27.53	21.82
SDA-MSE-LG	27.91	25.24
SDA-SURE-SM	27.90	25.24
SDA-SURE-SM-T	28.06	25.23

among all SDA results in Figure 1.

Table 2 shows quantitative results for Figure 1. SDA methods yielded up to 0.53 dB better PSNR (Peak Signal to Noise Ratio) than conventional BM3D for SD = 9.8%. Our proposed SDA-SURE-SM yielded almost the same performance to SDA-MSE-LG (only 0.01 dB difference). Since SURE based methods can utilize the data without ground truth, we also performed SURE based SDA with training data as well as testing data. SDA-SURE-SM-T yielded 0.15 dB and 0.16 dB better than SDA-MSE-LG and SDA-SURE-SM, respectively. Therefore, it seems that using test data for training SURE based denoiser is helpful to improve denoising performance.

For high noise level (SD = 19.6%), deep learning based approaches seem to have an advantage in denoising performance over BM3D significantly as shown in Figure 2. All SDA based methods clearly outperform conventional BM3D visually, while it is indistinguishable for the simulation results of all SDA methods with different cost function and various training set. These observations were confirmed by the quantitative results shown in Table 2. All SDA based methods outperformed BM3D significantly, but there were very small differences among all SDA methods, even when using noisy test data.

4.3. Regularization Effect of SDA

SDA was also trained to minimize the MSE between output and input noisy image to explore its regularization effects (SDA-REG). In case of the noise level of SD = 19.6%, early stopping was applied when the network started to overfit the noisy dataset after the first few epochs. The performance of this method was significantly worse than all the other methods with PSNR of 25.07 dB (SD = 9.8%) and 19.85 dB (SD = 19.6%) which is about 2 dB lower than PSNR of conventional BM3D. Noise patterns are visible as shown in Figures 1 and 2. This shows that the good performance of the SDA does not arise just from its structure, but comes from optimizing MSE and SURE.

4.4. Accuracy of Monte-Carlo SURE Approximation

A small value must be assigned to ϵ in (6) for accurate estimation of SURE. Ramani *et al.* have observed that

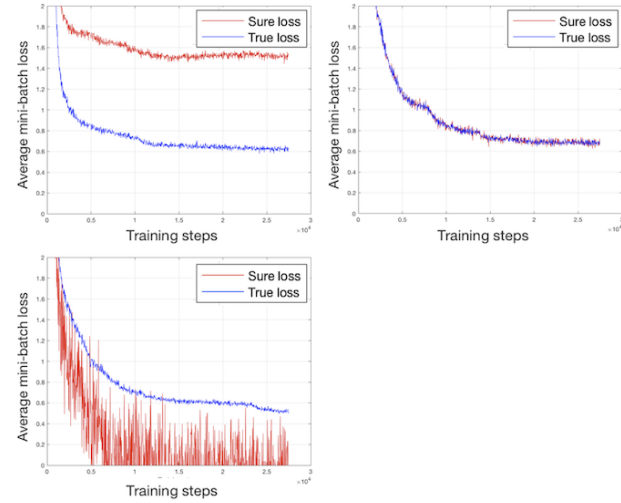


Figure 3. Loss curves for the training SDA with MSE (blue) and its corresponding Monte-Carlo SURE (red) using different ϵ , $\epsilon = 1$ (top left), $\epsilon = 10^{-5}$ (top right) and $\epsilon = 10^{-9}$ (bottom left). Monte-Carlo SURE well approximates true MSE for a wide range of ϵ .

ϵ can take a wide range of values and its choice is not critical (Ramani *et al.*, 2008). The admissible range of ϵ , however, depends on $h_i(y; \theta)$. According to our preliminary experiments for SDA with MNIST dataset, any choice for ϵ in between $[10^{-2}, 10^{-7}]$ worked well so that the SURE approximation with noisy data matches close to the MSE cost function with the ground truth data during training as illustrated in Figure 3 (top right). Extremely small values $\epsilon < 10^{-8}$ result in numerical instabilities as illustrated in Figure 3 (bottom left). On the contrary, when $\epsilon > 10^{-1}$, the approximation in (6) becomes inaccurate. Note, that these values are only for SDA trained with MNIST dataset. A suitable ϵ value must be carefully selected for other cases.

4.5. Results: CIFAR-10 Dataset

In this work, U-Net (Ronneberger *et al.*, 2015) was chosen to denoise the corrupted images from CIFAR-10 dataset for the same two noise levels of SD = 9.8% and SD = 19.6%. U-Net was modified so that it inputs RGB images with the dimension (32,32,3), which go through contractive path until reaching the size of (8,8,128) and then go through expansive path back to its original size. U-Net structure consists of skip connections, batch normalization layers and padded 3×3 convolutional layers followed by ReLU nonlinearities. The network also incorporates 3×3 maxpooling for downsampling and transposed convolution of size 3×3 and stride 2 for upsampling.

The dataset of 60,000 images was split into 58,000 training, 1900 validation and 100 test images. Training was done with Adam optimizer with batch size of 200 over 150 epochs. the initial learning rate of 0.001 which was dropped to 0.0001



Figure 4. Results of various denoising methods. From the top left, original image, noisy image ($SD = 9.8\%$, row 1, center), BM3D (row 1, right), UNET-MSE-LG (row 2, left), UNET-SURE-SM (row 2, center), UNET-SURE-SM-T (row 2, right).

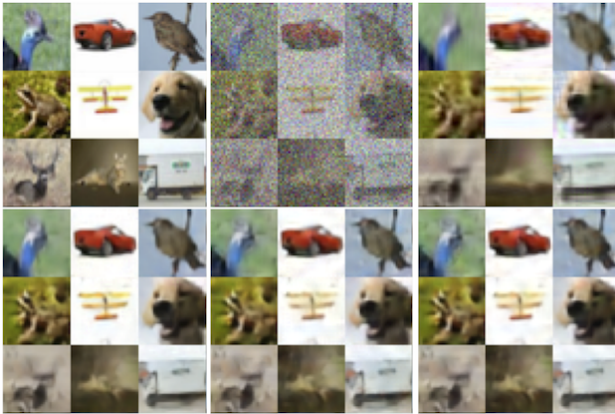


Figure 5. Results of various denoising methods. From the top left, original image, noisy image ($SD = 19.6\%$, row 1, center), BM3D (row 1, right), UNET-MSE-LG (row 2, left), UNET-SURE-SM (row 2, center), UNET-SURE-SM-T (row 2, right).

after 100 epochs. The ϵ value in (6) was set to 0.0001.

Figure 4 shows the denoising results for noise level of $SD=9.8\%$. UNET-MSE-LG method yields relatively cleaner images, while the denoising results of BM3D look slightly blurry. UNET-SURE methods seem to have similar results to UNET-MSE. In Figure 5 results for higher noise level ($SD=19.6\%$) are shown. It can be clearly seen that, UNET-MSE and UNET-SURE have significantly better denoising results than BM3D.

Table 3 displays the quantitative results for Figures 4 and 5. For the noise levels of $SD=9.8\%$ and 19.6% , all deep learning based denoising methods yielded $0.38 - 0.67$ dB and $0.53 - 1.05$ dB better PSNR than BM3D, respectively. UNET-MSE-LG outperformed other methods as expected (with ground truth data). UNET-SURE-SM-T also yielded comparable performance to UNET-MSE-LG. Using test data

Table 3. Denoising results of deep learning based denoisers with different training methods and data for CIFAR (performance in dB). MSE based UNET denoisers yielded comparable to or better than SURE based UNET denoisers as well as conventional state-of-the-art denoiser (BM3D).

METHOD	SD = 9.8%	SD = 19.6%
BM3D	28.16	24.40
UNET-MSE-LG	28.83	25.45
UNET-SURE-SM	28.54	24.93
UNET-SURE-SM-T	28.65	24.93

for training SURE based method did improve performance of it, but unlike MNIST simulation, UNET-SURE-SM-T was not able to outperform UNET-MSE-LG. For high noise, using both training and test data for SURE yielded almost the same performance as using training data only. This observation is consistent with MNIST simulation.

4.6. Results: High Resolution Natural Images

To show the capabilities of SURE based deep learning denoisers, we investigated a deeper and more powerful denoising network called DnCNN (Zhang et al., 2017a) for high resolution images. DnCNN consists of 17-layers of CNN with batch normalization and ReLU activation functions. Each convolutional layer has 64 filters of size 3×3 . Following (Zhang et al., 2017a), the network was trained with 400 images of size 180×180 and In total 1772×128 image patches of size 40×40 were extracted randomly from those images. For testing 12 widely used images were chosen in (Dabov et al., 2007). For DnCNN-SURE-SM-T, additional 326×128 image patches were extracted from those 12 noisy test images and were added to the training dataset. For all cases, the network was trained for 50 epochs with the noise level of $SD = 9.6\%$. Adam optimizer was used with the initial learning rate of 0.001 and then decayed to 0.0001 after 40 epochs.

DnCNN uses residual learning where the network is forced to learn the difference between noisy and ground truth images. Then, the output residual image was subtracted from the input noisy image to yield the estimated image. Therefore, for the case of residual learning, our network was trained with SURE using (15) as follows:

$$h(y; \theta) = y - \text{CNN}_\theta(y) \quad (15)$$

where $\text{CNN}_\theta(\cdot)$ is the DnCNN that is being trained using residual learning.

On a NVidia Titan X GPU, the training process took approximately 9 hours for DnCNN-MSE-LG and about 13 hours for DnCNN-SURE-SM. SURE based method take more training time than MSE based method because of the additional divergence term calculations done to optimize Monte-Carlo SURE cost function. For DnCNN-SURE-SM-T method, it took around 15 hours to complete the training

due to larger dataset.

For DnCNN, selection of the ϵ value in (6) turned out to be important for denoising performance. Stable training with good performance was possible when selecting $\epsilon = 0.001$. However, the network trained with $\epsilon = 0.0001$ took much more epochs to converge and yielded lower final PSNR. On the other hand, the training process became unstable for $\epsilon = 0.01$ and the network usually diverged after 20 epochs.

Table 4 presents denoising performance using BM3D (Dabov et al., 2007), state-of-the-art deep CNN (DnCNN) image denoiser trained with MSE (Zhang et al., 2017a) and the same DnCNN image denoiser trained with SURE without knowing noiseless ground truth images for different dataset variations (as described in Table 1). MSE based DnCNN image denoiser, DnCNN-MSE-LG, yielded the best denoising performance over other methods such as BM3D, which is consistent with the results in (Zhang et al., 2017a). Our DnCNN-SURE-SM yielded better performance than BM3D for 7 images among 12, but worse performance for 5 images. On average, DnCNN-SURE-SM was able to achieve comparable performance to BM3D. Better performance for SURE based method was achieved when the training dataset was augmented with the noisy test images. As a result, DnCNN-SURE-SM-T were able to outperform the conventional BM3D and DnCNN-SURE-SM.

Figure 6 illustrates example images that DnCNN with SURE outperformed BM3D. BM3D has an advantage for high denoising performance when images contain repeated structures or simple large flat areas. Examples in Figure 6 seem to have quite complicated non-repeated structures, so that DnCNN with SURE yielded better denoising results than BM3D. BM3D consistently yielded slightly blurrier images

Table 4. Results of BM3D, deep CNN image denoiser with MSE and the same deep CNN image denoiser with Monte-Carlo SURE (performance in dB). SURE based image denoiser yielded comparable results to MSE based image denoiser and BM3D.

IMAGE	BM3D	MSE	SURE	SURE-T
C. MAN	29.47	30.03	29.61	29.75
HOUSE	33.00	33.13	32.41	32.64
PEPPERS	30.23	30.69	30.38	30.57
STARFISH	28.58	29.83	28.96	29.08
MONARCH	29.35	30.36	29.94	30.10
AIRPLANE	28.37	29.08	28.81	28.89
PARROT	28.89	29.40	29.11	29.22
LENA	32.06	32.28	31.82	32.04
BARBARA	30.64	29.91	28.82	29.02
BOAT	29.78	30.02	29.70	29.83
MAN	29.60	30.01	29.78	29.87
COUPLE	29.70	30.01	29.56	29.72
AVERAGE	29.97	30.40	29.91	30.06

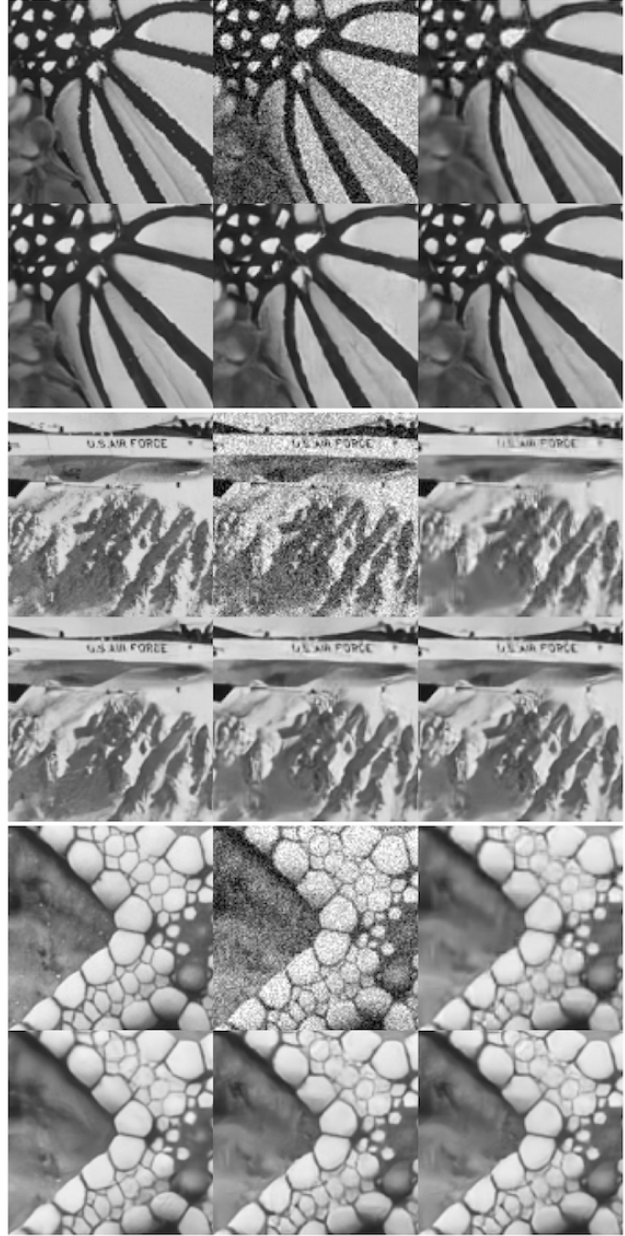


Figure 6. Results of various denoising methods. Top: ‘Monarch’ image, Middle: ‘Airplane’ image, Bottom: ‘Starfish’ image. For each image, there are 6 image patches where from the top left corner, original (row 1, left), noisy (row 1, center), BM3D (row 1, right), DnCNN-MSE-LG (row 2, left), DnCNN-SURE-SM (row 2, center), and DnCNN-SURE-SM-T (row 2, right). In these images, DnCNN-SURE-SM outperformed BM3D.

than other deep learning based denoisers possibly due to rare patch effect (BM3D uses Wiener filter for rare patches). In contrast, Figure 7 illustrates example images that BM3D outperformed DnCNN with SURE. These images contain repeated pattern structures (‘Barbara’ image) or simple flat areas (‘House image’). Since BM3D looks for similar image patches for denoising, repeated patterns can be a key factor

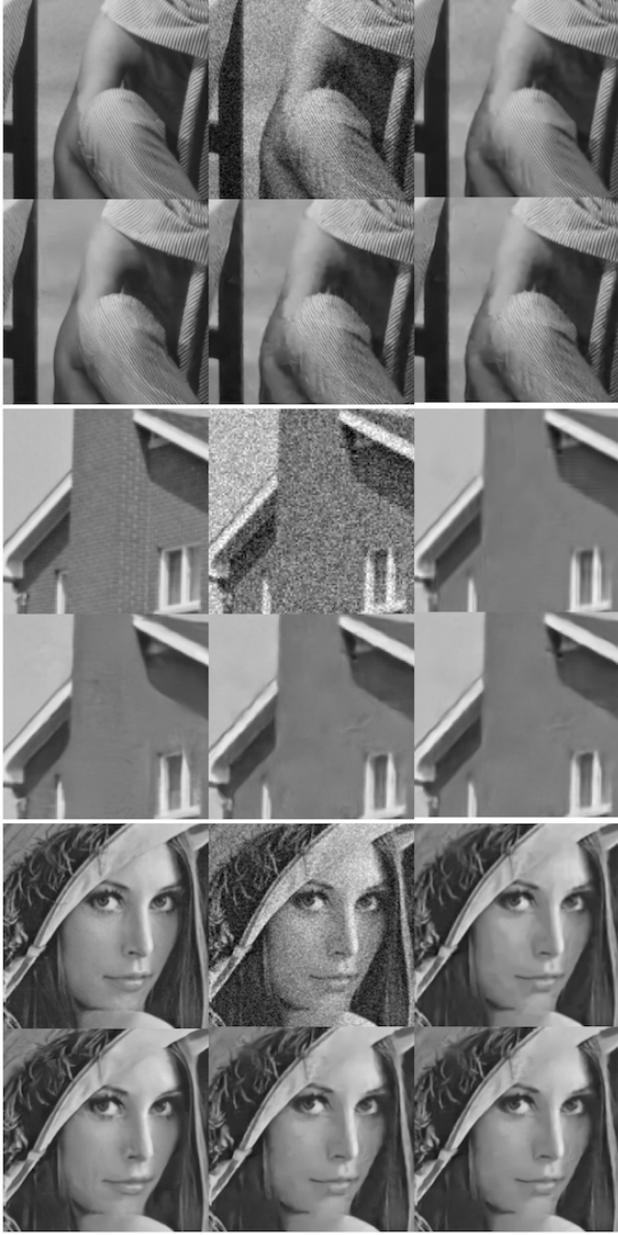


Figure 7. Results of various denoising methods. Top: ‘Barbara’ image, Middle: ‘House’ image, Bottom: ‘Lena’ image. For each image, there are 6 image patches where from the top left corner, original (row 1, left), noisy (row 1, center), BM3D (row 1, right), DnCNN-MSE-LG (row 2, left), DnCNN-SURE-SM (row 2, center), and DnCNN-SURE-SM-T (row 2, right). In these images, DnCNN-SURE-SM outperformed BM3D.

to yield strong denoising results. Note that for ‘Barbara’ image with repeated textures, BM3D even outperformed DnCNN with MSE. These preliminary results suggest that it is possible to train state-of-the-art deep learning based denoisers using SURE based optimization criteria without noiseless ground truth images so that good denoising performance can be achieved, better than BM3D.

5. Discussion

We proposed a Monte-Carlo SURE based training method for general deep learning denoisers. Our proposed method train denoisers without noiseless ground truth data such that they have comparable denoising performance to the conventional state-of-the-art BM3D or to the same denoisers that are trained with noiseless data. Our SURE based training method does not only work for simple SDA (Vincent et al., 2010), but also works for U-NET (Ronneberger et al., 2015) and state-of-the-art DnCNN denoising network (Zhang et al., 2017a) without noiseless ground truth images.

In this work, Gaussian noise with known variance was assumed in all simulations. However, there are several noise estimation methods that can be used with SURE (see (Ramanu et al., 2008) for more details). SURE based methods can incorporate a variety of noise distributions other than Gaussian noise. For example, SURE for Poisson noise has been used for parameter selection of conventional filter (Deledalle et al., 2010). Generalized SURE for exponential families has been proposed (Eldar, 2009) so that other common noise in imaging systems can be potentially considered for SURE based methods. Note that SURE does not require any prior knowledge on images, so it can be applied to the measurement domain. For example, some measurement domain in medical imaging follows Poisson distribution (CT, PET, SPECT) and there are other measurement domain that contains complex Gaussian noise (MRI).

In medical imaging, there is no known exact noise distribution. The noise property of medical imaging in image domain is complex, but there have been some works to analyze it so that it approximately follows weighted Gaussian distribution (Barrett et al., 1994; Fessler, 1996; Gravel et al., 2004). Since SURE expression is the sum of all unbiased risk estimator for each pixel, it is trivial to apply SURE locally with spatially varying variance. However, due to correlation in noise of image domain (through radon transform for CT or PET, or through Fourier transform for MRI), it will be challenging to apply SURE to image domain directly.

Our proposed SURE based deep learning denoiser can potentially be useful for applications with massive amount of noisy images, but with few noiseless images or with expensive noiseless images. Deep learning based denoising research is still evolving, it may be even possible to achieve significantly better performance than BM3D or other conventional state-of-the-art denoisers with our SURE based training method. Further investigation will be needed for high performance denoising networks.

Acknowledgements

This work was partly supported by Basic Science Research Program through the National Research Foundation of

Korea(NRF) funded by the Ministry of Education(NRF-2017R1D1A1B05035810) and the Technology Innovation Program or Industrial Strategic Technology Development Program (10077533, Development of robotic manipulation algorithm for grasping/assembling with the machine learning using visual and tactile sensing information) funded by the Ministry of Trade, Industry & Energy (MOTIE, Korea).

References

Abadi, Martín, Barham, Paul, Chen, Jianmin, Chen, Zhifeng, Davis, Andy, Dean, Jeffrey, Devin, Matthieu, Ghemawat, Sanjay, Irving, Geoffrey, Isard, Michael, Kudlur, Manjunath, Levenberg, Josh, Monga, Rajat, Moore, Sherry, Murray, Derek G., Steiner, Benoit, Tucker, Paul, Vasudevan, Vijay, Warden, Pete, Wicke, Martin, Yu, Yuan, and Zheng, Xiaoqiang. Tensorflow: A system for large-scale machine learning. In *Proceedings of the 12th USENIX Conference on Operating Systems Design and Implementation*, pp. 265–283, 2016.

Barrett, H H, Wilson, D W, and Tsui, B M. Noise properties of the EM algorithm: I. Theory. *Physics in Medicine and Biology*, 39(5):833–846, May 1994.

Blu, T and Luisier, F. The SURE-LET Approach to Image Denoising. *IEEE Transactions on Image Processing*, 16(11):2778–2786, October 2007.

Bottou, Léon. Online Learning and Stochastic Approximations. In *On-line learning in neural networks*, pp. 9–42. Cambridge University Press New York, NY, USA, 1998.

Buades, A, Coll, B, and Morel, J M. A review of image denoising algorithms, with a new one. *Multiscale Modeling & Simulation*, 4(2):490–530, January 2005.

Burger, Harold C, Schuler, Christian J, and Harmeling, Stefan. Image denoising: Can plain neural networks compete with BM3D? In *IEEE Conference on Computer Vision and Pattern Recognition (CVPR)*, pp. 2392–2399, 2012.

Chen, Hu, Zhang, Yi, Kalra, Mannudeep K, Lin, Feng, Chen, Yang, Liao, Peixi, Zhou, Jiliu, and Wang, Ge. Low-Dose CT With a Residual Encoder-Decoder Convolutional Neural Network. *IEEE Transactions on Medical Imaging*, 36(12):2524–2535, November 2017.

Chen, Liang-Chieh, Papandreou, George, Kokkinos, Iasonas, Murphy, Kevin, and Yuille, Alan L. Semantic image segmentation with deep convolutional nets and fully connected crfs. In *International Conference on Learning Representation (ICLR)*, 2015.

Dabov, Kostadin, Foi, Alessandro, Katkovnik, Vladimir, and Egiazarian, Karen. Image denoising by sparse 3-D transform-domain collaborative filtering. *IEEE Transactions on Image Processing*, 16(8):2080–2095, August 2007.

Deledalle, C A, Tupin, F, and Denis, L. Poisson NL means: Unsupervised non local means for Poisson noise. In *IEEE International Conference on Image Processing (ICIP)*, pp. 801–804, 2010.

Eldar, Y C. Generalized SURE for Exponential Families: Applications to Regularization. *IEEE Transactions on Signal Processing*, 57(2):471–481, January 2009.

Fessler, J A. Mean and variance of implicitly defined biased estimators (such as penalized maximum likelihood): applications to tomography. *IEEE Transactions on Image Processing*, 5(3):493–506, 1996.

Gao, Ruohan and Grauman, Kristen. On-demand learning for deep image restoration. In *IEEE International Conference on Computer Vision (ICCV)*, 2017.

Girshick, R, Donahue, J, and Darrell, T. Rich feature hierarchies for accurate object detection and semantic segmentation. In *IEEE Conference on Computer Vision and Pattern Recognition (CVPR)*, pp. 580–587, 2014.

Gravel, P, Beaudoin, G, and DeGuise, J A. A Method for Modeling Noise in Medical Images. *IEEE Transactions on Medical Imaging*, 23(10):1221–1232, October 2004.

He, Kaiming, Zhang, Xiangyu, Ren, Shaoqing, and Sun, Jian. Deep Residual Learning for Image Recognition. In *IEEE Conference on Computer Vision and Pattern Recognition (CVPR)*, pp. 770–778, 2016.

Kang, Eunhee, Min, Junhong, and Ye, Jong Chul. A deep convolutional neural network using directional wavelets for low-dose X-ray CT reconstruction. *Medical Physics*, 44(10):e360–e375, October 2017.

Kingma, Diederik P and Ba, Jimmy. Adam - A Method for Stochastic Optimization. In *International Conference on Learning Representation (ICLR)*, 2015.

Krizhevsky, A, Sutskever, I, and Hinton, G E. Imagenet classification with deep convolutional neural networks. In *Advances in Neural Information Processing Systems (NIPS) 25*, pp. 1097–1105, 2012.

LeCun, Yann, Bengio, Yoshua, and Hinton, Geoffrey. Deep learning. *Nature*, 521(7553):436–444, May 2015.

Lefkimiatis, Stamatios. Non-local Color Image Denoising with Convolutional Neural Networks. In *IEEE Conference on Computer Vision and Pattern Recognition (CVPR)*, pp. 5882–5891, 2017.

Long, Jonathan, Shelhamer, Evan, and Darrell, Trevor. Fully convolutional networks for semantic segmentation. In *IEEE Conference on Computer Vision and Pattern Recognition (CVPR)*, pp. 3431–3440, 2015.

Mao, Xiao Jiao, Shen, Chunhua, and Yang, Yu Bin. Image restoration using very deep convolutional encoder-decoder networks with symmetric skip connections. In *Advances in Neural Information Processing Systems (NIPS) 29*, pp. 2810–2818, 2016.

Nesterov, Yurii. A method of solving a convex programming problem with convergence rate $o(1/k^2)$. In *Soviet Mathematics Doklady*, 1983.

Ramani, S, Blu, T, and Unser, M. Monte-Carlo Sure: A Black-Box Optimization of Regularization Parameters for General Denoising Algorithms. *IEEE Transactions on Image Processing*, 17(9):1540–1554, August 2008.

Ren, Shaoqing, He, Kaiming, Girshick, Ross, and Sun, Jian. Faster R-CNN: Towards real-time object detection with region proposal networks. In *Advances in Neural Information Processing Systems (NIPS) 28*, pp. 91–99, 2015.

Ronneberger, Olaf, Fischer, Philipp, and Brox, Thomas. U-Net: Convolutional Networks for Biomedical Image Segmentation. In *International Conference on Medical Image Computing and Computer-Assisted Intervention (MICCAI)*, pp. 234–241, 2015.

Salmon, J. On Two Parameters for Denoising With Non-Local Means. *IEEE Signal Processing Letters*, 17(3):269–272, March 2010.

Stein, C M. Estimation of the mean of a multivariate normal distribution. *The Annals of Statistics*, 9(6):1135–1151, November 1981.

Van De Ville, D and Kocher, M. SURE-Based Non-Local Means. *IEEE Signal Processing Letters*, 16(11):973–976, November 2009.

Van De Ville, Dimitri and Kocher, Michel. Nonlocal Means With Dimensionality Reduction and SURE-Based Parameter Selection. *IEEE Transactions on Image Processing*, 20(9):2683–2690, August 2011.

Vincent, Pascal, Larochelle, Hugo, Lajoie, Isabelle, Bengio, Yoshua, and Manzagol, Pierre Antoine. Stacked denoising autoencoders: Learning Useful Representations in a Deep Network with a Local Denoising Criterion. *Journal of Machine Learning Research*, 11:3371–3408, December 2010.

Wang, Yan, Zhang, Pei, An, Le, Ma, Guangkai, Kang, Jiayin, Shi, Feng, Wu, Xi, Zhou, Jiliu, Lalush, David S, Lin, Weili, and Shen, Dinggang. Predicting standard-dose PET image from low-dose PET and multimodal MR images using mapping-based sparse representation. *Physics in Medicine and Biology*, 61(2):791–812, January 2016.

Wang, Yi-Qing and Morel, Jean-Michel. Can a Single Image Denoising Neural Network Handle All Levels of Gaussian Noise? *IEEE Signal Processing Letters*, 21(9):1150–1153, May 2014.

Wolterink, Jelmer M, Leiner, Tim, Viergever, Max A, and Isgum, Ivana. Generative Adversarial Networks for Noise Reduction in Low-Dose CT. *IEEE Transactions on Medical Imaging*, 36(12):2536–2545, November 2017.

Xie, Junyuan, Xu, Linli, and Chen, Enhong. Image denoising and inpainting with deep neural networks. In *Advances in Neural Information Processing Systems (NIPS) 25*, pp. 341–349, 2012.

Zhang, Kai, Zuo, Wangmeng, Chen, Yunjin, Meng, Deyu, and Zhang, Lei. Beyond a Gaussian Denoiser: Residual Learning of Deep CNN for Image Denoising. *IEEE Transactions on Image Processing*, 26(7):3142–3155, May 2017a.

Zhang, Kai, Zuo, Wangmeng, Gu, Shuhang, and Zhang, Lei. Learning Deep CNN Denoiser Prior for Image Restoration. In *IEEE Conference on Computer Vision and Pattern Recognition (CVPR)*, pp. 3929–3938, 2017b.